

10-20-92
1.1.1

Final Report
Microgravity Science and Applications Division
Fluid Physics Program

The Circular Hydraulic Jump in Microgravity

NASA Grant NAG 3-1627

Principal Investigator: C. Thomas Avedisian
Sibley School of Mechanical and Aerospace Engineering
Cornell University
193 Grumman Hall
Ithaca, New York 14853-7501
phone: 607-255-5105
FAX: 607-255-1222
email: cta2@cornell.edu

Period: June 24, 1994 to June 23, 1996

Cost: ~~XXXXXXXXXX~~

Abstract

This report summarizes the key experimental results and observations that were obtained under NASA grant NAG 3-1627 from the Fluid Physics Program. The Principle Investigator was Thomas Avedisian. In addition a half-time post-doctoral associate, Ziqun Zhao, was funded for half year. The project monitor was David Chao of the NASA-Lewis Research Center in Cleveland, Ohio. The grant period was originally for one year at \$34K and a no-cost extension was applied for and granted for an additional year.

The research consisted of an experimental study of the circular hydraulic jump (CHJ) in microgravity using water as the working fluid. The evolution of the CHJ radius was measured during a sudden transition from normal to microgravity in a drop tower. The downstream height of the CHJ was controlled by submerging the target plate in a tank filled with water to the desired depth, and the measurements are compared with an existing theory for the location of the CHJ.

Results show that the CHJ diameter is larger in microgravity than normal gravity. The adjustment of the CHJ diameter to a sudden change in gravity occurs over a period of about 200ms for the conditions of the present study, and remains constant thereafter for most of the flow conditions examined. For flow conditions that a CHJ was not first established at normal gravity but which later appeared during the transition to microgravity, the CHJ diameter was not constant during the period of microgravity but continually changed. Good agreement between measured and predicted CHJ radii is found for normal gravity CHJ radii, but comparatively poorer agreement is observed for the CHJ radii measurements in microgravity.

1. Objectives

The purpose of this project was to study liquid jet impingement in microgravity. The emphasis was on the hydraulic jump phenomenon. The objectives were the following:

- 1) record the evolution of a circular hydraulic jump (CHJ) upon a transition from Earth normal gravity ($G=1$) to microgravity, $G \ll 1$ [†];
- 2) make quantitative measurements of the CHJ diameter in microgravity;
- 3) measure the curvature of the free liquid surface across the CHJ during the transition from normal to microgravity; and
- 4) compare the CHJ diameter measurements with published predictions.

Figure 1 is a schematic diagram that shows the basic features of an impinging liquid jet that undergoes a hydraulic jump. The parameters were the liquid flow rate, jet orifice diameter, and the downstream liquid height.

The decision to focus on the transition from $G=1$ to $G \ll 1$ was made because of the available experimental run time of just over 1s as discussed in Section 3. The transition of the CHJ from normal to microgravity was considered to be the easiest way to document gravity's effect on the CHJ without pursuing a more extensive study of liquid jet impingement in which the jet would first be established in microgravity.

2. Importance of the Circular Hydraulic Jump

Impingement of a circular liquid jet onto a surface is important in a variety of processes: impingement cooling of electronic devices, materials in manufacturing processes, laser mirrors, and aircraft generator coils; and vapor absorption refrigeration cycles. A feature of impinging liquid jets is their potential for dissipating high heat transfer rates. For example, the highest steady state heat fluxes reported in any configuration were achieved by a water jet impinging onto a plasma heated surface (Liu and Lienhard 1993). A concern for jet impingement is the potential for the formation of a circular hydraulic jump downstream of which the liquid velocity, and thus heat transfer, are

[†] $G \equiv g/g_0$ where $g_0 \approx 9.8 \text{ m/s}^2$. In the remaining text, the designation ' $G=1$ ' means Earth's normal gravity and ' $G \ll 1$ ' means 'microgravity' which for the proposed experiments will mean any G value in the range $10^{-4} < G < 10^{-2}$ based on the drop tower package used (Avedisian et al. 1988)

reduced. It is, therefore, important to predict the location of the CHJ (the jump diameter, D_h) and the parameters upon which it depends to avoid the reduction of heat transfer. Gravity figures prominently in both the location of a CHJ and the curvature of the free liquid surface across the jump. The CHJ occurs where the expanding liquid jet undergoes a transition from a 'supercritical' to a 'subcritical' flow, in the sense of a suitably defined Froude number being greater or less than unity, respectively.

Existing formulations (see Section 5.2) for predicting D_h (Middleman 1995) show that as gravity is reduced D_h should increase. As a result, heat transfer rates may be extended in microgravity to larger diameter. Our results confirm this general trend, though quantitative agreement is not demonstrated. The flow downstream of a CHJ in microgravity is significantly different from the downstream flow at $G=1$. Capillary waves form in the downstream flow in $G \ll 1$ and a more gradual transition across the jump occurs from the toe of the jump (see fig. 1) to the downstream flow. The origin of these waves is speculated to be due in part to the rapid increase in curvature created by the sudden transition from $G=1$ to $G \ll 1$ which we demonstrate in this report, or, as speculated by Hornung et al. (1995), to vorticity generation at the CHJ.

This proposal was envisioned to be the first part of a larger effort on liquid jet impingement in microgravity that would have included fluid mechanics and heat transfer. In the first part, described in this report, experiments to characterize the fluid mechanics of an impinging jet in microgravity were carried out. The primary focus was on measuring the evolution of D_h during the transition from $G=1$ to $G \ll 1$: the surface curvature across the CHJ, film thickness across the CHJ, and D_h were measured. The second (future) part was to continue these isothermal measurements and to pursue a study of heat transfer to an impinging liquid jet in microgravity.

3. Brief Review of Prior Work

An extensive literature exists on jet impingement in general, and the hydraulic jump in particular. Standard fluid mechanic textbooks provide basic formulations for planar inviscid hydraulic jumps (e.g., Allen and Ditsworth 1972; Fox and McDonald 1992). For the CHJ, Nirapathdongporn (1968) reviews the literature prior to 1968. Errico (1986) reviews some of the

later theories and presents measurements of the CHJ diameter at $G=1$ which show various degrees of agreement with analyses. The role of surface tension on stabilization of the CHJ jump surface at $G=1$ was discussed by Liu and Lienhard (1993), who showed that increasing the fluid height downstream of the jump increased the effect of surface tension at the free liquid surface.

A suitably defined Froude number, $Fr = U/c$ where 'c' is the appropriate wave speed (e.g., $c=(gh)^{1/2}$ from 'shallow water' theory (Milne-Thomson 1979, p. 443) is an indicator for the expectation of a hydraulic jump. Above a critical value, Fr_c , in the sense of the mean liquid velocity exceeding the wave speed, a CHJ will always occur at some radial location in the expanding jet. While $Fr_c=1$, a non-unity critical Froude number has been argued (Rahman et al. 1991b) to be dependent on the velocity profile used for the analysis of the CHJ.

A number of numerical and analytical studies have predicted the behavior of the CHJ at $G=0$. Laminar (Rahman et al. 1990, 1991a; Thomas et al. 1990) and turbulent (Rahman et al. 1991) jets have been analyzed and predicted to be free of a hydraulic jump at $G=0$. In the vicinity of a jump at $G=1$, back-flow, separation, and eddies are observed in experimental studies and predicted in early treatments of the problem (e.g., Craik et al. 1981; Tani 1948). No analogous observations have been reported for $G \ll 1$. A 'classic' analysis by Watson (1964) results in a closed-form solution to the laminar momentum and continuity equations for the CHJ radius where an inviscid approximation is made for the stagnation region and the flow downstream of the jump, the flow is self-similar upstream of the CHJ, and the limit of an infinite Froude number is assumed. Some failures of the model are analyzed by Bowles and Smith (1992) who extend the analysis to finite Fr and predict the film thickness shape near the jump. Numerical solutions by Chaudhry (1994) accounts for the effect of turbulence and heat transfer and provide predictions of both the CHJ diameter and film thickness downstream of the jump.

One experimental study is known on the problem of jet impingement at $G \ll 1$ (Labus 1976). The focus was on studying the shapes assumed by a free liquid surface rolling off of the edge of a plate on which a liquid impinged. A drop tower was used to create the microgravity environment. A hint of what to expect for the CHJ diameter at $G \ll 1$ was noted by the observation

of Labus (1976) that no CHJ occurred during any of the $G \ll 1$ tests while they were a common occurrence at $G=1$ for nominally the same flow conditions. Reducing gravity thus appears to push the CHJ off the target plate for the flow conditions examined.

4. Experimental Design

A microgravity environment for the present experiments was created by using a drop tower. Central to the success was the ability to observe all desired features of the flow within the available experimental run time. It was anticipated that the reaction time of the CHJ radius to sudden changes in G would be much less than the available experimental time (on the order of 1s for the facility used). While this was verified for most of the conditions analyzed, for some it was not as discussed in the next section.

The basic CHJ visualization set-up is shown in fig. 2. It consists of a flow-loop with the following components: recirculating pump; plenum containing beads and a flow straightener (to dampen the inlet flow - see fig. 3) and a removable orifice plate attached at one end; plexiglas chamber within which the target plate is mounted; flow control valve; and cameras and lighting. The height of the liquid level downstream of the jump is controlled by partially submerging the target plate by raising the water level to the desired height above the plate. The experimental conditions examined were the following. The downstream fluid height, h_{∞} , was 2.0 mm, 4.0 mm, 6.0 mm, 10.0 mm, or 15.0 mm. The liquid flow rates were 2.39ml/s, 6.32ml/s, 9.93ml/s, or 26.47ml/s. To create laminar jets, a sharp-edged orifice was used. Orifice diameters of 1.22mm, 2.56mm and 3.83mm were used. They were machined into a stainless steel plate that could be bolted to the bottom of the plenum (see fig. 3). The plenum was mounted such that the orifice was 7.62cm above the target surface. The diameter of the liquid jet, D_j , at a reference $2D_j$ above the target surface was measured directly.

The target plate was a 6.35 mm thick and 23 cm diameter pyrex glass disk. It was painted black on its back to reduce light reflection. The glass disk was attached to a plexiglass support disk 1.9 cm thick and 23 cm I.D. and mounted to one end of a circular plexiglass cylinder that was then bolted to the containment vessel and sealed with o-rings. A mirror tilted to 45° under the circulation

tank (see fig. 2) allowed for observations of the underside of the jet. This view was a primary one to measure the CHJ radius. Additional viewing angles were along the plane through the liquid to show the cross-sectional profile shape of the liquid film across the CHJ, and an angled top view for global features of the CHJ. The working fluid was water at room temperature in all the experiments.

To keep the design simple, the primary means of data acquisition was photographic. A 35mm Nikon F3 camera with MD-4 motor drive (operated at 5 frames/s or 200ms intervals) and attached 105 mm NIKKOR macro lens was used to record images at all three camera positions. Approximately five 35mm exposures were obtained in the period of $G \ll 1$. Video images using a COHU CCD camera (30 images/s) with attached 28mm NIKKOR macro lens were used to record the evolution of the CHJ in the transition to microgravity, and 30 video images were obtained. All cameras and lenses were securely mounted to prevent damage by the shock of the impact. Lighting was provided by halogen lamps. The CHJ diameter was measured from the video images of underneath views using a 'video caliper' (Video Caliper 306, Colorado Video Inc.) placed on the video monitor that was calibrated with a precision ruler (Schaedler Quinzel, Inc., USA) added to the image. Side views (from the 35mm camera) were used to obtain the cross-sectional shape of the liquid film across the CHJ. The side view images were fed into a MAC-based data acquisition system (AUTOMATIX Image Analysis Program) and an operator-selected gray scale was used to identify the various boundaries involved. A 19.05 mm diameter ball bearing image converted the side view pixel count to length with a precision of about $\pm 66 \mu\text{m}$.

The experimental procedure was as follows. Flow conditions were first set so that a CHJ existed at $G=1$ (several conditions were also examined in which a CHJ did not exist at $G=1$ but which later appeared during the transition to $G \ll 1$). The instrumentation package was then released into free fall by deactivating the magnet which initially held the package to the support ceiling. With the various cameras in operation, features of the impinging jet were then recorded during the flight of the package. Analysis of the photographic images was done as per above.

5. Discussion of Results

5.1 Visualization

Fig. 5 shows two representative photographs of a CHJ. The upper photograph is for a jet at $G=1$ and the lower photograph shows the same jet 400ms into the period of $G \ll 1$. The downstream fluid depth is 4 mm and the flow rate is 9.32ml/s. As is typical of jet impingement, the upstream flow is a thin film which transitions to the downstream fluid depth over a short distance at the CHJ. At $G \ll 1$, the downstream flow shows a series of concentric capillary waves that do not exist at $G=1$. The transition of the flow across the jump is more gradual at $G \ll 1$ than at $G=1$ and the liquid boundary at the CHJ appears to be pushed outward.

Fig. 6 shows a sequence of photographs of the change of the free surface across the jump at five different times (spaced by 200ms) during the period just prior to microgravity ($G=1$) and into microgravity ($G \ll 1$). The vertical line is the jet. The change of curvature across the jump is clearly shown in fig. 6. After entering microgravity, the jump moves outward from the stagnation point and the jump curvature increases. The source of the downstream waves in $G \ll 1$ is due to the abrupt increase of radius of curvature when gravity transitions from $G=1$ to $G \ll 1$. It remains to show that a flow downstream of a CHJ in microgravity would not exhibit this behavior if the CHJ were first established in microgravity. This question will require a longer experimental flight time.

Fig. 7 shows bottom view photographs depicting the increase of the CHJ diameter in microgravity relative to normal gravity. In these photographs the jet is directed outward toward the plane of the viewer. The circular capillary waves are also shown in fig. 7.

The effect of downstream fluid height, h_∞ , on the CHJ is shown in the series of photographs in fig. 8. For $h_\infty=2$ mm and $Q = 6.32$ ml/s, a smooth jump with minimal downstream disturbance is seen. During the transition to $G \ll 1$ an abrupt change of curvature occurs at the toe of the jump which forms a large wave in the downstream flow that appears like a 'hump'. This effect is also shown in fig. 9 which is in the sequence of fig. 5 taken 200ms into $G \ll 1$. At $h_\infty=4$ mm and $Q = 6.32$ ml/s (fig. 8) the increase in CHJ diameter is also evident, as is the thinning of the downstream flow due to the increase in curvature.

At lower flow rates, the CHJ moves closer to the stagnation point. This effect is shown in fig. 10. For $h_\infty = 2$ mm (fig. 10) the capillary waves exist even at normal gravity (compare with

fig. 8). At 4 mm and 2.39ml (fig. 8) the jump is very close to the stagnation point but the surface of the downstream flow appears very turbulent. Since in $G \ll 1$ the surface curvature across the jump increases - the transition across the jump is more gradual - the primary fluid effect of G appears to be in the hydrostatic pressure of the downstream flow. This point is discussed further in the next section.

5.2 Quantitative Measurements of the CHJ Diameter.

Measurements of the evolution of the CHJ diameter were made from the video images using a computer-based analysis system. Figs. 11 shows the effect of flow rate on the CHJ at two different flow rates for the 2.56 mm diameter orifice and $h_\infty = 4$ mm. At $t < 0$ s, $G = 1$ and a steady CHJ exists. At $t = 0$ s, the instrumentation package is released into free fall and the period of microgravity begins. As shown from the measurements in fig. 11, enough time appears to exist for the CHJ to reach a steady position at $G \ll 1$.

The effect of jet diameter on the CHJ is shown in fig. 12. Increasing the jet diameter pushes the CHJ outward. The adjustment of the CHJ to microgravity is clearly shown and again occurs on a time shorter than the available run time of about 1.2s.

The effect of downstream fluid height on the CHJ diameter is shown in fig. 13 at both normal and microgravity. The lines shown in the figure are placed to suggest trends. At normal gravity, D_h decreases as h_∞ increases. This effect is speculated to be due to the increase of hydrostatic pressure in the downstream flow as h_∞ increases which would tend to increase the inwardly directed radial pressure on the downstream side of the jump. The jump moves inward where the fluid velocity will be higher to re-establish a balance of momentum across the jump. For $G \ll 1$, however, there is no clear trend of CHJ diameter with h_∞ . If the hydrostatic pressure of the downstream flow is predicted to effect D_h but measured trends with h_∞ are not predicted for $G \ll 1$, it may be that wall shear in the downstream flow which is neglected in the analysis is in fact important in $G \ll 1$. For $G = 0$ D_h should be infinite so the small but non zero gravity level in the present experiments may unmask the role of friction in the downstream flow on D_h .

While this investigation was focused on experiment, the plethora of analyses of the

hydraulic jump motivated applying some of these analyses to the data obtained during this investigation. Most of the published analysis has been associated with 'planar' jumps. For the CHJ, comparatively little work has been reported. Middleman (1995) reviews some of the theories.

A simplified viewpoint of the origin of a CHJ is of a flow slowed by friction at the wall (and the increasing flow area due to the radial geometry) until a point is reached at which the flow cannot adjust to the changing downstream conditions without experiencing a 'jump' in film thickness to satisfy mass conservation. In another theory, the liquid jet is assumed to expand under the influence of an adverse gravitational pressure gradient and will eventually separate (Tani 1948) as a result of a nonlinear interaction between the wall shear stress, surface tension and the pressure gradient across the film (Bowles and Smith 1992; Gaudier and Smith 1983). This interaction leads to an upstream influence and the CHJ is the result that allows an adjustment of the flow to downstream conditions.

The earliest, and most often quoted, analyses of a CHJ assume that the upstream and downstream flows are inviscid. Applying a mass and momentum balance across a control volume that includes the CHJ (see fig.), and a force balance across the free surface of the jump, results in a relation between D_h , curvature of the free surface, κ , ($=1/R$ where R is the radius of curvature of the fluid across the jump) and flow parameters as

$$\left(\frac{Q}{\pi D_h}\right)^2 \left(\frac{1}{h} - \frac{1}{h_\infty}\right) = \frac{1}{2} g_0 (h_\infty^2 - h^2) G \quad 1$$

and

$$R = \frac{1}{\kappa} \approx \frac{\sigma}{\rho G g_0 h_\infty} \quad 2$$

where 'R' is the radius of curvature and κ is the curvature. From eq. 1 as G decreases, D_h increases; and, for given G , $D_h \propto 1/h_\infty^2$. From eq. 2, $\kappa \propto G$. The effect of G on D_h and κ is

qualitatively verified by the data shown in figs 11, 12, and 14 in which D_h is larger in microgravity than normal gravity, and the curvature across the jump is less in microgravity than normal gravity. At $G=0$, D_h is infinite by eq. 1 and thus should not be observed, but this limit is an impractical one because of the impossibility of experimentally creating precisely the $G=0$ condition.

Since G changes abruptly in the present experiments, the sudden decrease in κ can be the source of waves that are clearly evident in fig. 5, 8, and 10 for $h_\infty=2\text{mm}$ and $t=0.2\text{s}$ in the downstream flow in microgravity.

The qualitative trend of how D_h depends on h_∞ for given G that is predicted by eq. 1 is not confirmed by the $G \ll 1$ measurements reported here. Fig. 13 shows that D_h exhibits at most a weak variation with h_∞ as h_∞ increases in $G \ll 1$ while eq. 1 shows that D_h should asymptote to infinity as G is reduced. This limit G is not followed by the measurements and the discrepancy could be due to neglecting friction.

An extension of eq. 1 to include friction in the upstream fluid was first reported by Watson (1964) who uses a boundary layer model to predict the velocity profile across the upstream film. The results show that the flow becomes self-similar at some radial position away from the stagnation point. This theory has the essential features of more advanced treatments (e.g., Bowles and Smith 1992; Higuera 1994) and is applied to the present data. The result can be expressed in non-dimensional form by introducing the parameters (Middelman 1995) $Y \equiv RH/\text{Fr}_\infty + 1/(2RH)$, $R \equiv D_h/D_j \text{Re}^{-1/3}$, the Reynolds number $\text{Re} \equiv 4Q/(\pi D_j \nu)$, $H \equiv 2h_\infty/D_j \text{Re}^{1/3}$ and $\text{Fr}_\infty \equiv U_j^2/(Gg_0 h_\infty)$:

$$Y = .26/(R^3 + .287)$$

3

where the approximation $h_\infty \gg h$ has been made. The viscous limit is $R \rightarrow 0$ in eq. 3. Y and R are known from the experimental results: D_h as discussed previously, and h_∞ and Q as input parameters ($U_j = Q/[\pi D_j^2/4]$). A reference location of $2D_j$ above the target surface was used to measure D_j . For the water kinematic viscosity at 300°K we took $\nu \approx 8.95 \times 10^{-7} \text{m}^2/\text{s}$ (Keenan et al. 1969). An average G of 1.1×10^{-2} is used over the free-fall distance for the unshielded falling

package. Though eq. 3 is not explicit in the jump radius, it can be used to determine the extent of agreement between measured and predicted CHJ radii.

Fig. 15 shows the variation of Y with R . The inviscid limit (dotted line) clearly does not predict our measurements while all of the $G=1$ data are predicted reasonably well when viscosity effects are included (eq. 2). On the other hand all of the measurements of D_h for $G \ll 1$ are not well predicted by eq. 3. These observations suggest that a physical process which is masked at $G=1$ may become dominant at $G \ll 1$. Candidate processes include flow separation downstream of the jump and the nonuniform downstream velocity that is not included in the analysis, or neglect of viscous drag at the surface of the plate.

6. Conclusions

The major conclusions from this nominal one-year preliminary study are the following:

- 1) a steady CHJ can be established in microgravity;
- 2) the CHJ in microgravity is larger than at normal gravity, other flow conditions being the same;
- 3) the fluid response time to re-establish a CHJ at $G \ll 1$ from a jump at $G=1$ is on the order of 200ms;
- 4) the transition of the fluid film thickness across the CHJ boundary is more gradual in microgravity than at normal gravity due to the reduction in hydrostatic pressure in the downstream film;
- 5) the $G=1$ measurements are well correlated by an existing formulation but the microgravity measurements are not well predicted;
- 6) the CHJ diameter shows no clear trend with h_∞ in a microgravity environment; and
- 7) All $G \ll 1$ downstream flow patterns showed capillary ripples.

Publications/Presentations:

The Circular Hydraulic Jump in Microgravity, *Journal of Fluid Mechanics*, submitted

7. References

- Allen, T. and Ditsworth, R.L. (1972) *Fluid Mechanics*, pp. 291-291, McGraw-Hill, New York.
- Avedisian, C.T., Yang, J.C and Wang, C.H. (1988) *Proc. R. Soc. Lond A***420**, 183.
- Bowles, R.I. and Smith, F.T. (1992) *J. Fluid Mechanics*. **242**, 145.
- Chaudhury, Z.H. (1964) *J. Fluid Mechanics*. **20**, 501.
- Craik, A.D.D., Latham, R.C., Fawkes, M.J. and Gribbon, P.W.F. (1981) *J. Fluid Mechanics* **112**, 347.
- Errico, M. (1986) "A Study of the Interaction of Liquid Jets with Solid Surfaces," Ph.D. Thesis, University of California, San Diego.
- Fox, R.W. and McDonald, A.T. (1992) *Introduction to Fluid Mechanics*, 4th edition, pp. 525-530, John Wiley, New York.
- Gajjar, J.S.B. and Smith, F.T. (1983) *Mathematika* **30**, 77.
- Higuera, F.J. (1994) *J. Fluid Mechanics*. **274**, 69.
- Jackson, G.S. and Avedisian, C.T. (1994) *Proc. R. Soc. Lond.*, **A446**, 257-278.
- Keenan, J.H., Keys, F.G., Hill, P.G., and Moore, J.G. (1969) *Steam Tables* , p. 114, John Wiley, New York.
- Labus, T.L. (1976) "Liquid Jet Impingement Normal to a Disk in Zero Gravity," Ph.D. Thesis, University of Toledo.
- Liu, X. and Lienhard, J.H. (1993) *Exp. Fluids*, **15**, 108.
- Middelmann S. (1995) *Modeling Axisymmetric Flows*, Chapter 5, New York, Academic Press.
- Nirapathdongporn, S. (1968) "Circular Hydraulic Jump", M.Eng. Thesis, Asian Institute of Technology, Bangkok, Thailand.
- Thomas, S., Hankey, W.L., Faghri, A., and Rahman, M.M. (1990) *J. Heat Transf.* **112**, 728.
- Tani, I. (1948) *J. Phys. Soc. Japan* **4**, 212.
- Watson, E.J. (1964) *J. Fluid Mechanics* **20**, 481.

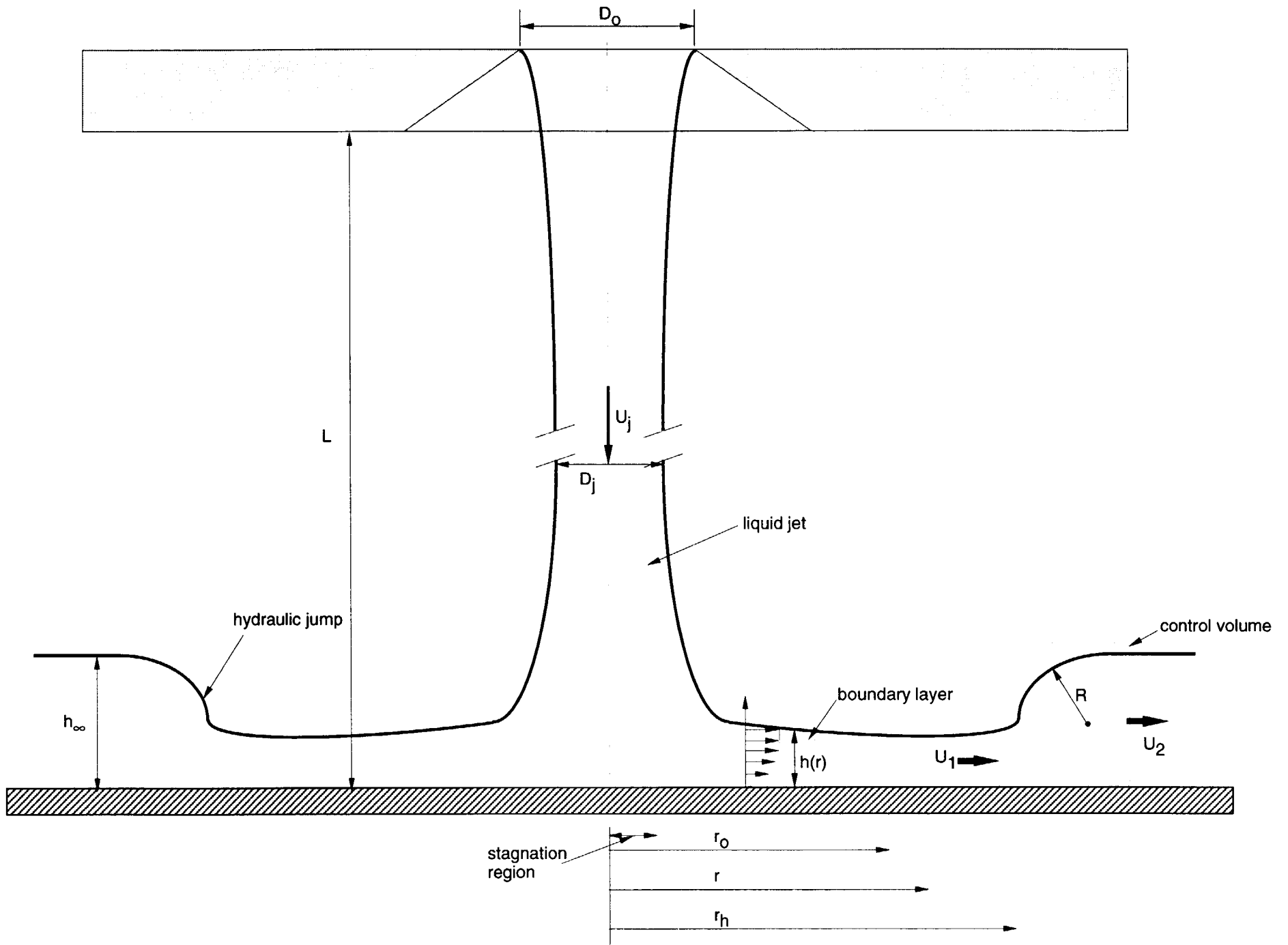


Figure 1

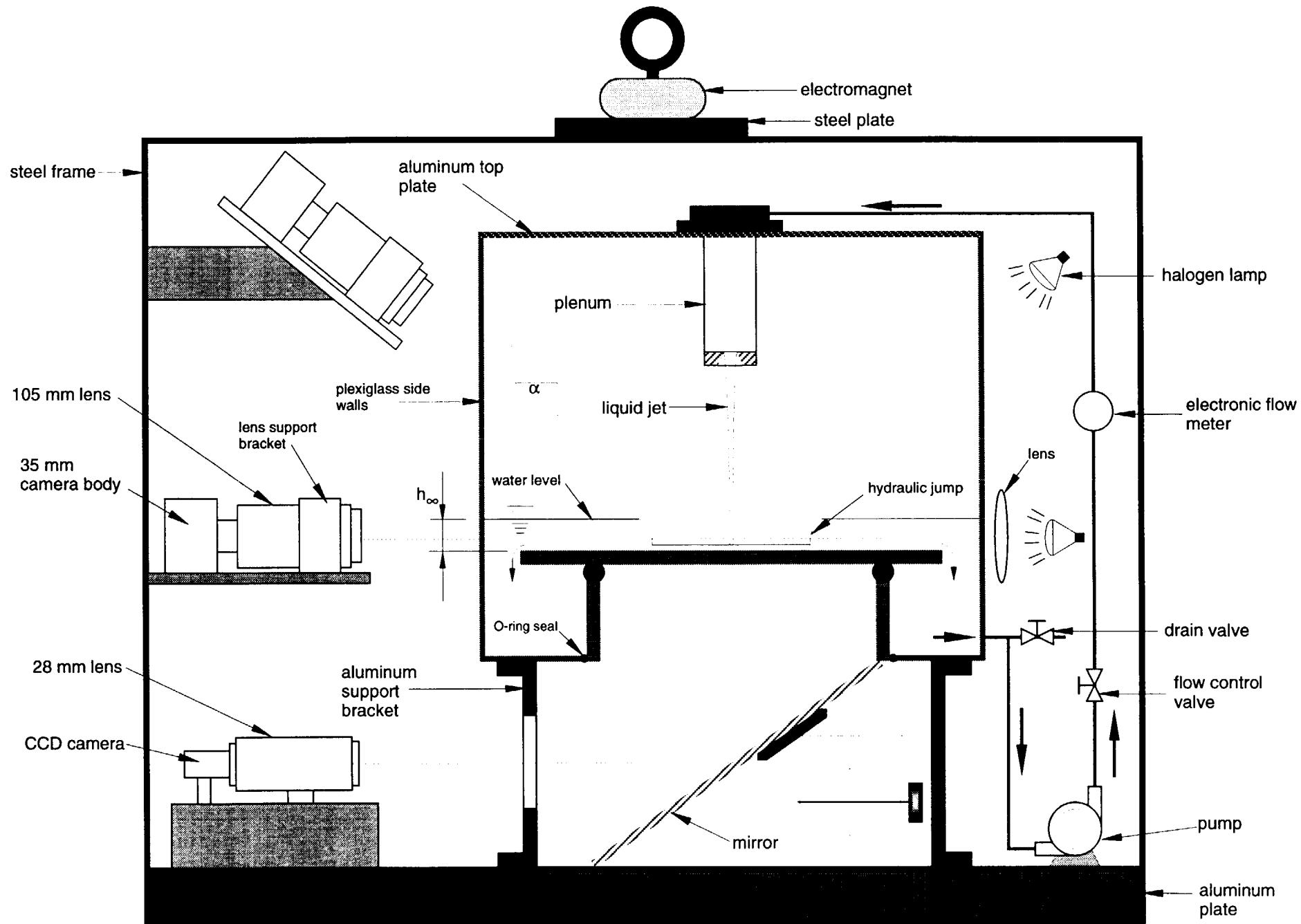
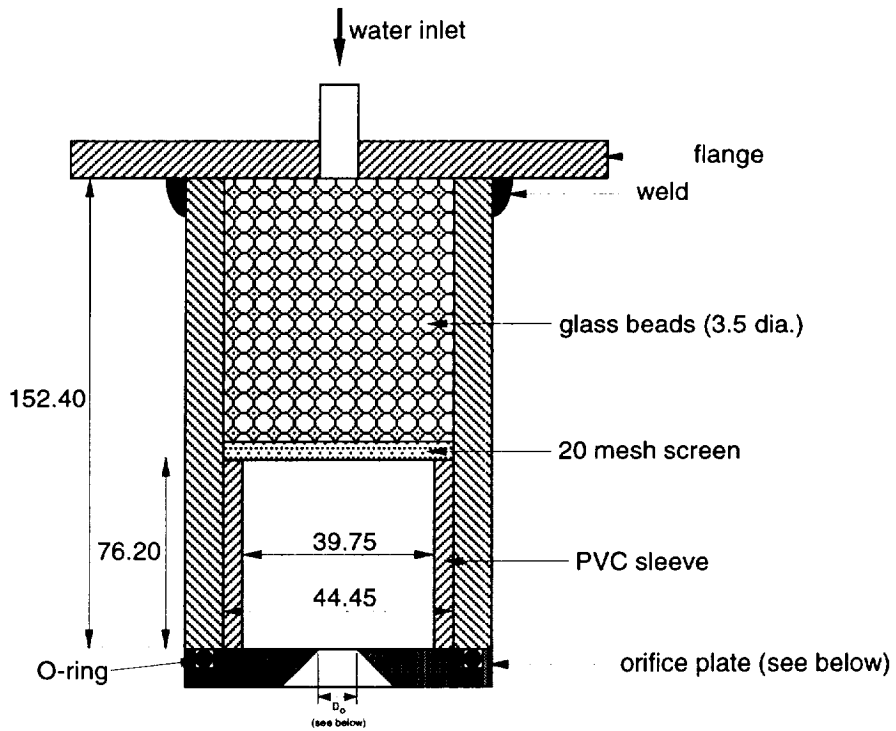
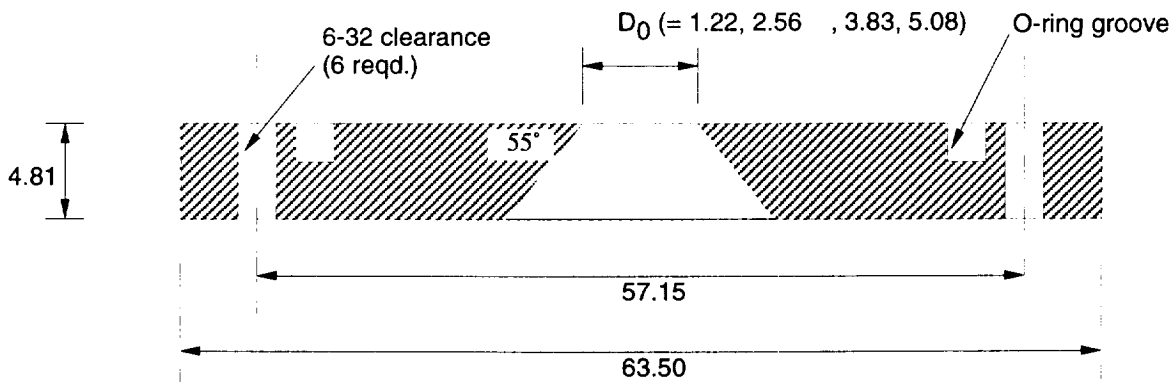


Figure 2



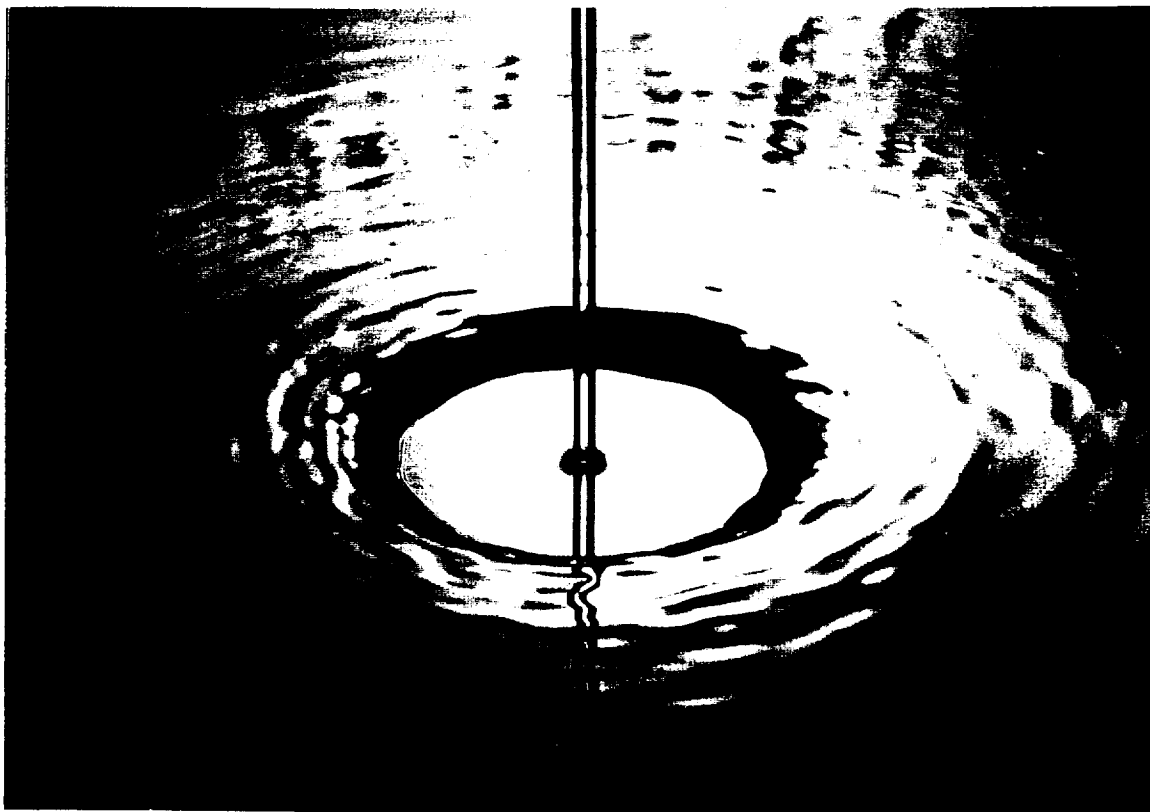
Plenum Design
[numbers in mm; not to scale]

Figure 3



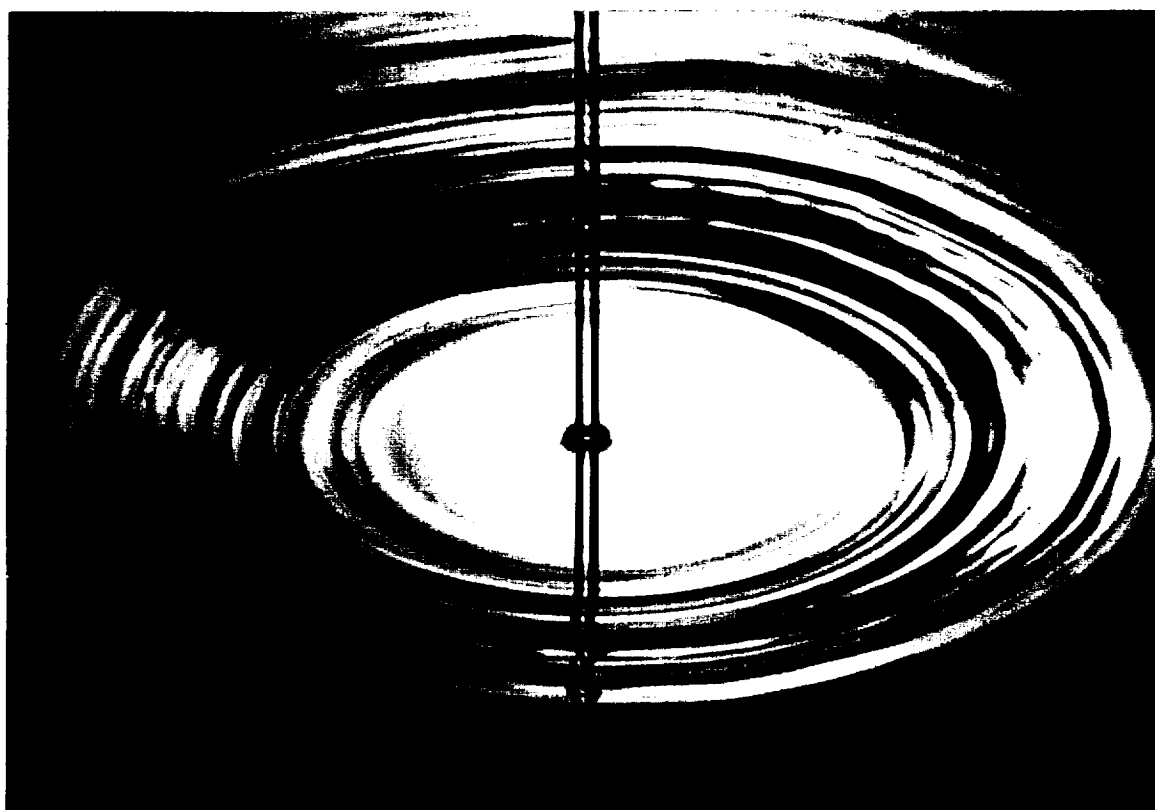
Detail of orifice plate
[numbers in mm; not to scale]

Figure 4



$G=1$; $h_{\infty}=4\text{mm}$; $Q=9.32\text{ml/s}$

(a)



$G \ll 1$

(b)

figure 5

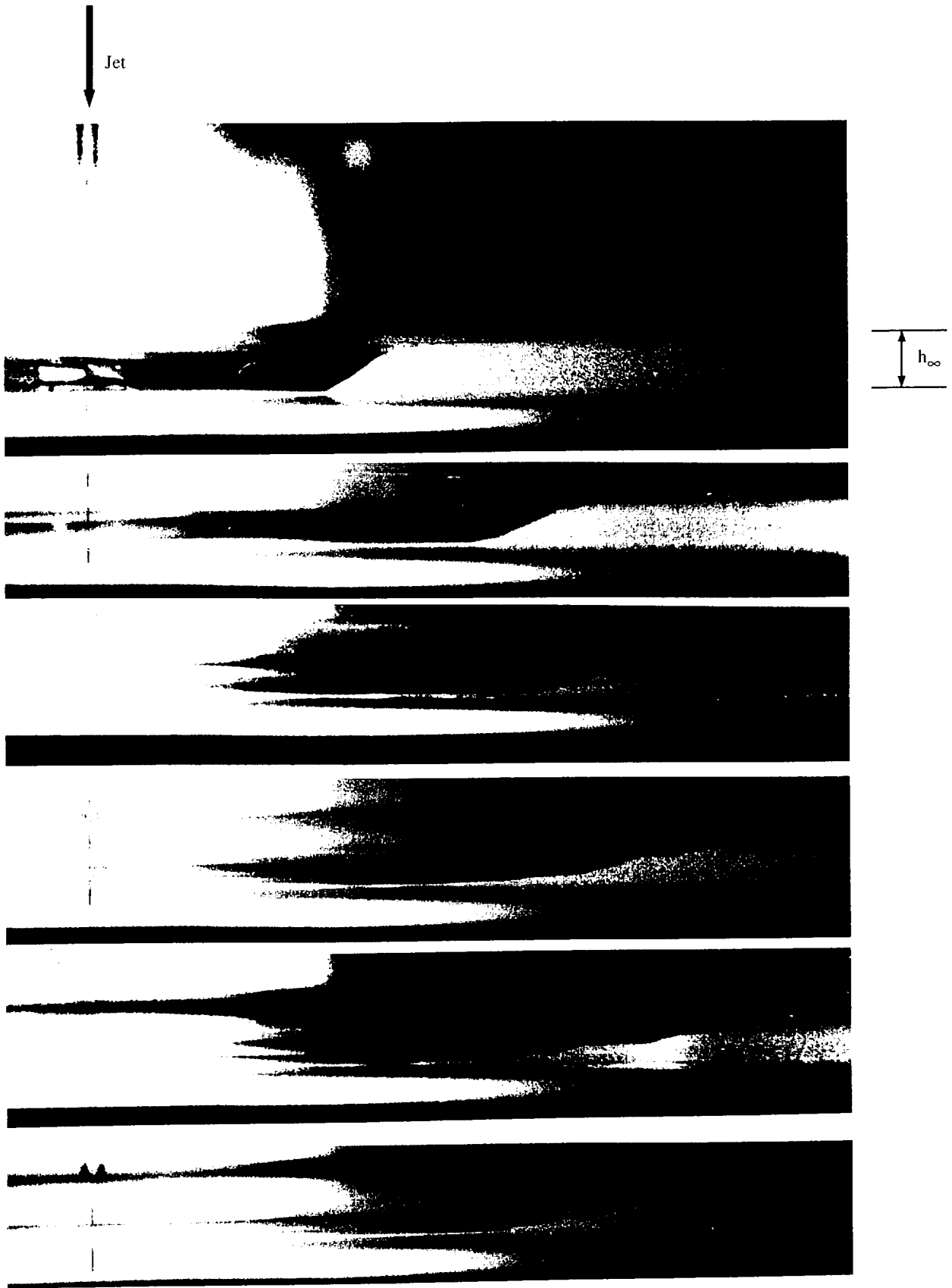
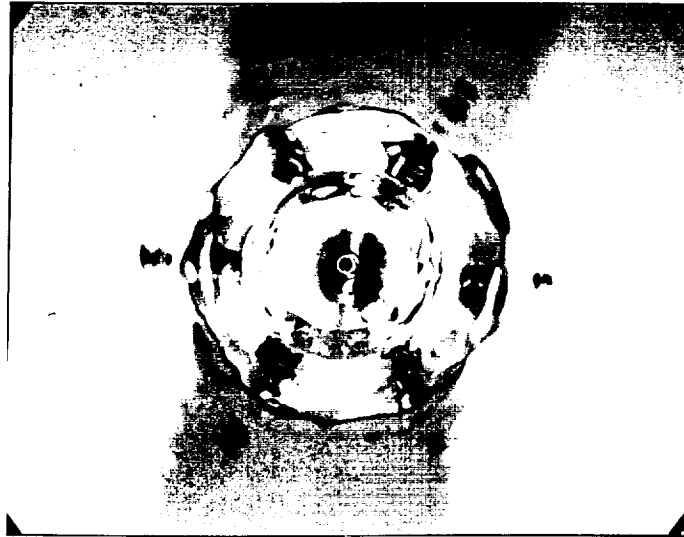


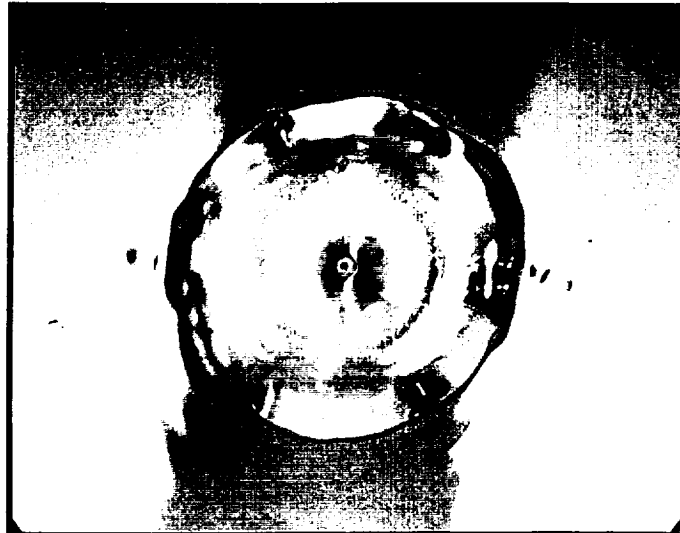
Figure 6

$D_0 = 2.56 \text{ mm}$ $Q = 9.932 \text{ ml/s}$ $h_\infty = 4 \text{ mm}$
(View from underneath target plate)

$t = 0$
 $G = 1$



$t = 0.2 \text{ sec}$
 $G \ll 1$



40 mm

$t = 0.4 \text{ sec}$
 $G \ll 1$

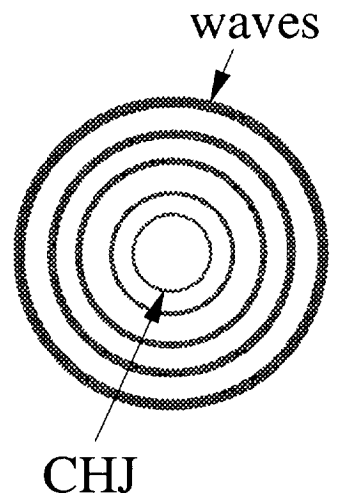
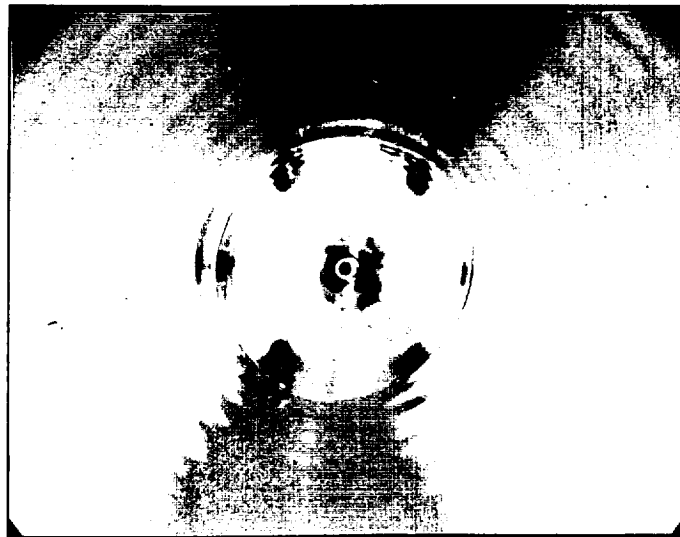


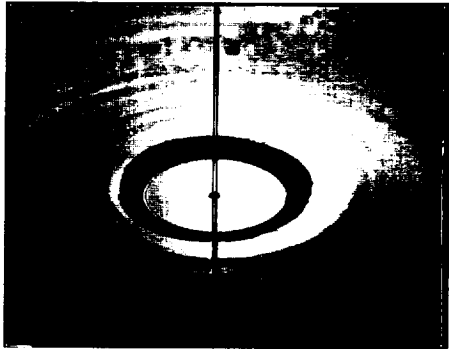
figure 7

$$D_0 = 1.22 \text{ mm}$$

$$Q = 6.32 \text{ ml/s}$$

$$h_\infty = 2 \text{ mm}$$

$$h_\infty = 4 \text{ mm}$$



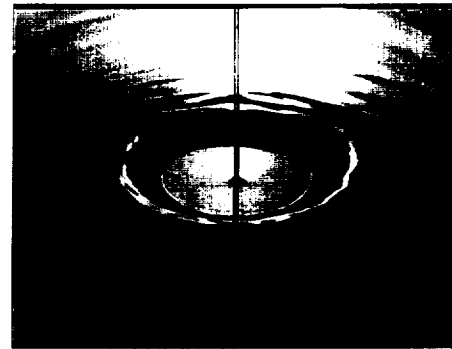
$t = 0$
 $G = 1$



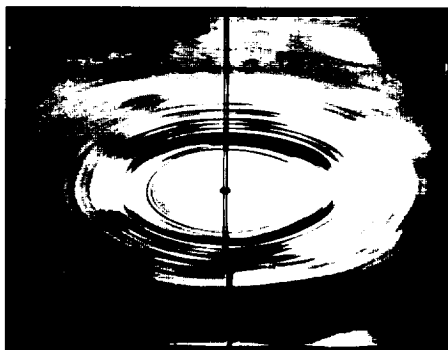
$t = 0$
 $G = 1$



$t = 0.2 \text{ sec}$
 $G \ll 1$



$t = 0.2 \text{ sec}$
 $G \ll 1$

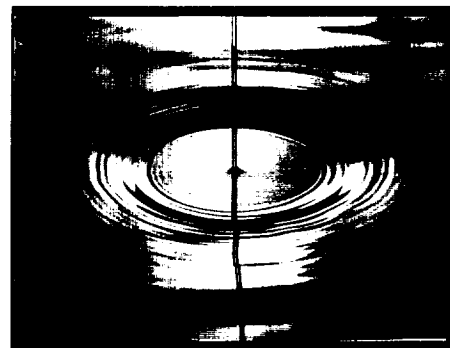


$t = 0.4 \text{ sec}$
 $G \ll 1$



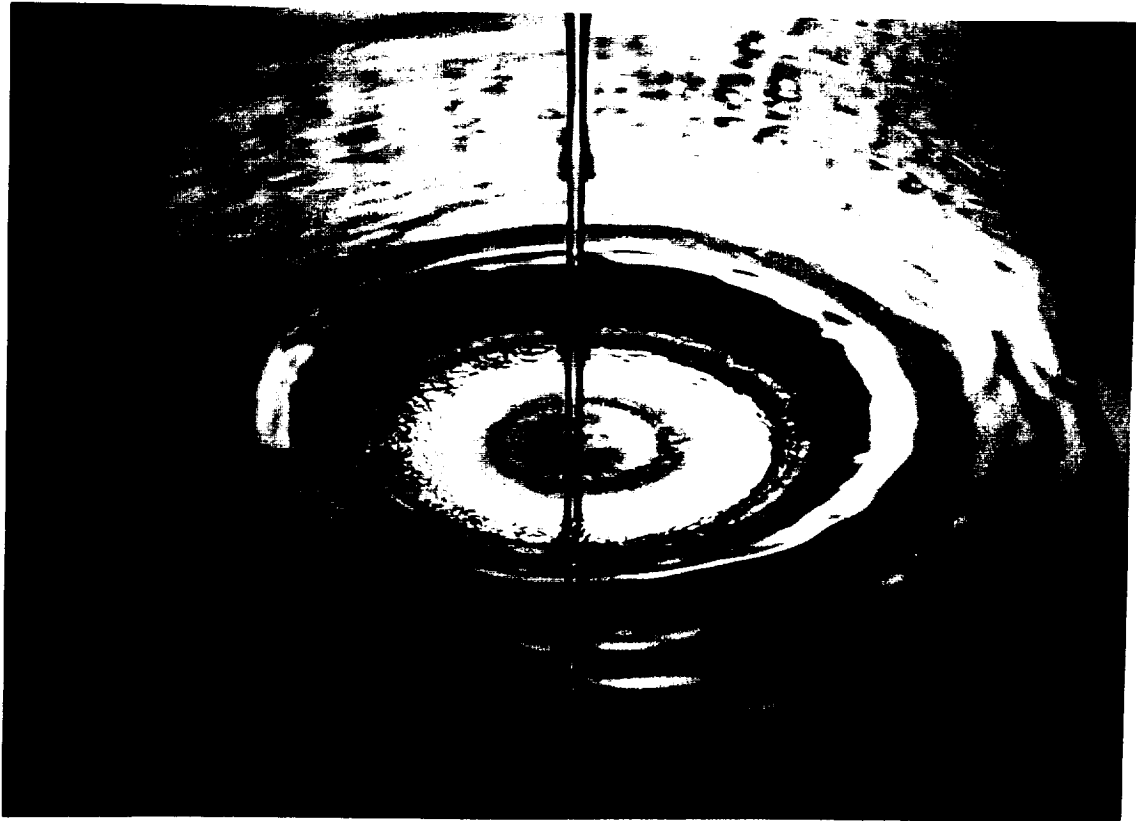
$t = 0.4 \text{ sec}$
 $G \ll 1$

40 mm



$t = 0.6 \text{ sec}$
 $G \ll 1$

figure 8



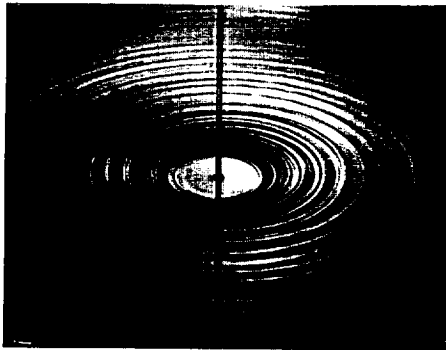
Photograph of a CHJ taken 200ms after the period of microgravity. The flow conditions are identical to figure 5. The 'hump' just downstream of the jump is caused by the rapid increase of curvature from $G=1$ to $G \ll 1$.

Figure 9

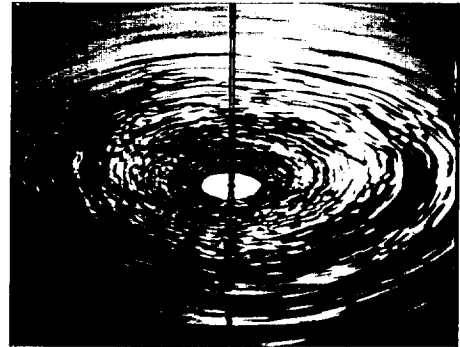
$$D_0 = 1.22 \text{ mm} \quad Q = 2.39 \text{ ml/s}$$

$$h_\infty = 2 \text{ mm}$$

$$h_\infty = 4 \text{ mm}$$

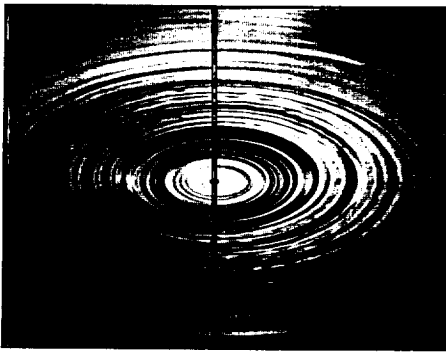


$t = 0$
 $G = 1$

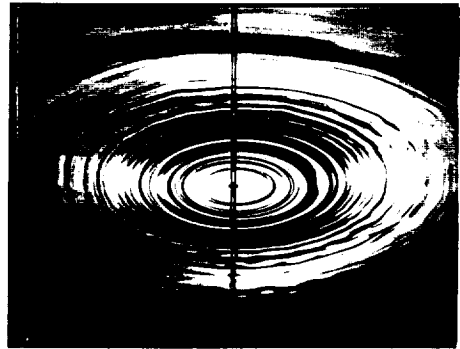


$t = 0$
 $G = 1$

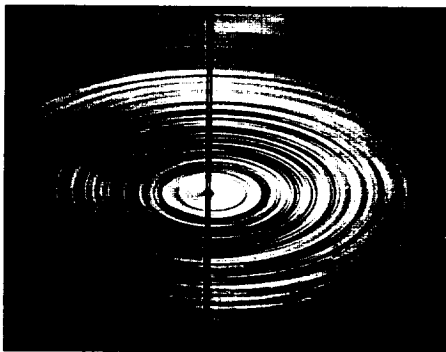
40 mm



$t = 0.2 \text{ sec}$
 $G \ll 1$



$t = 0.2 \text{ sec}$
 $G \ll 1$



$t = 0.4 \text{ sec}$
 $G \ll 1$



$t = 0.4 \text{ sec}$
 $G \ll 1$

figure 10

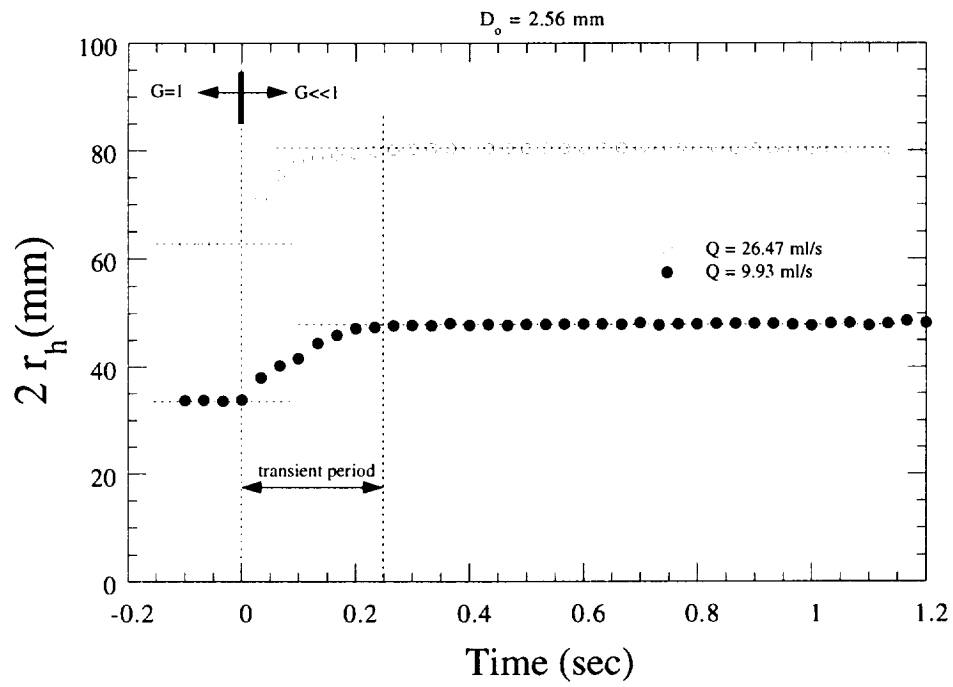
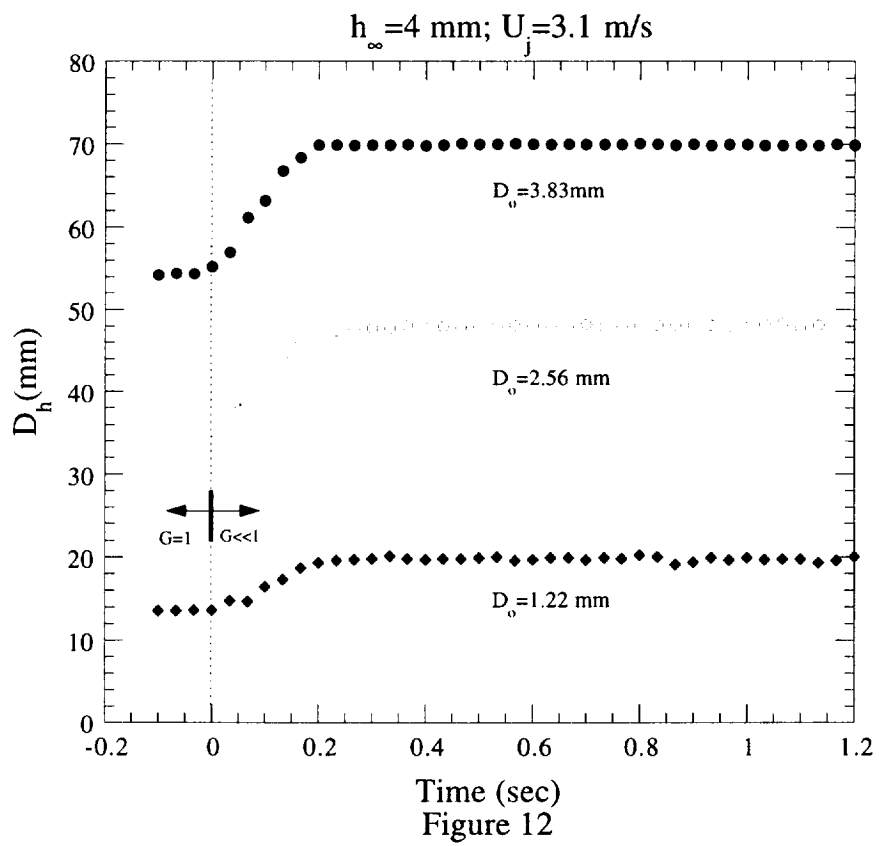


Figure 11



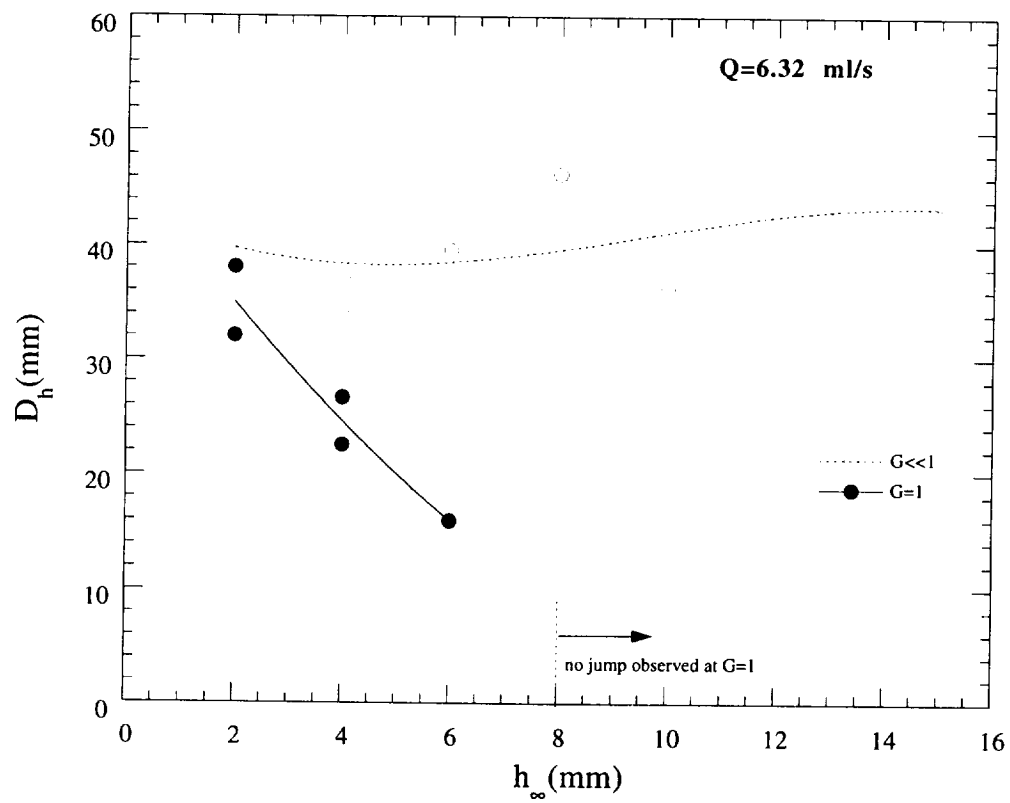


Figure 13

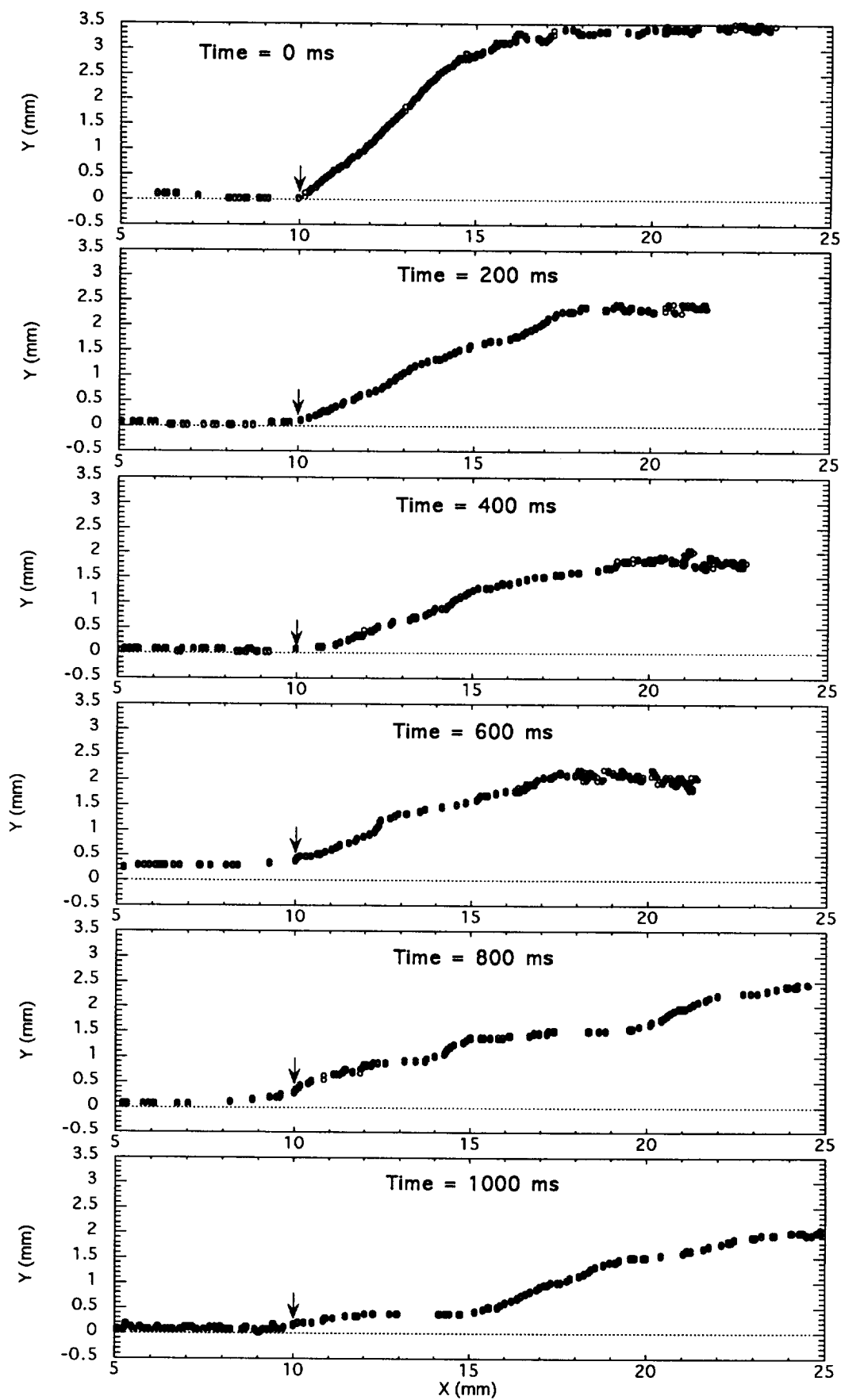
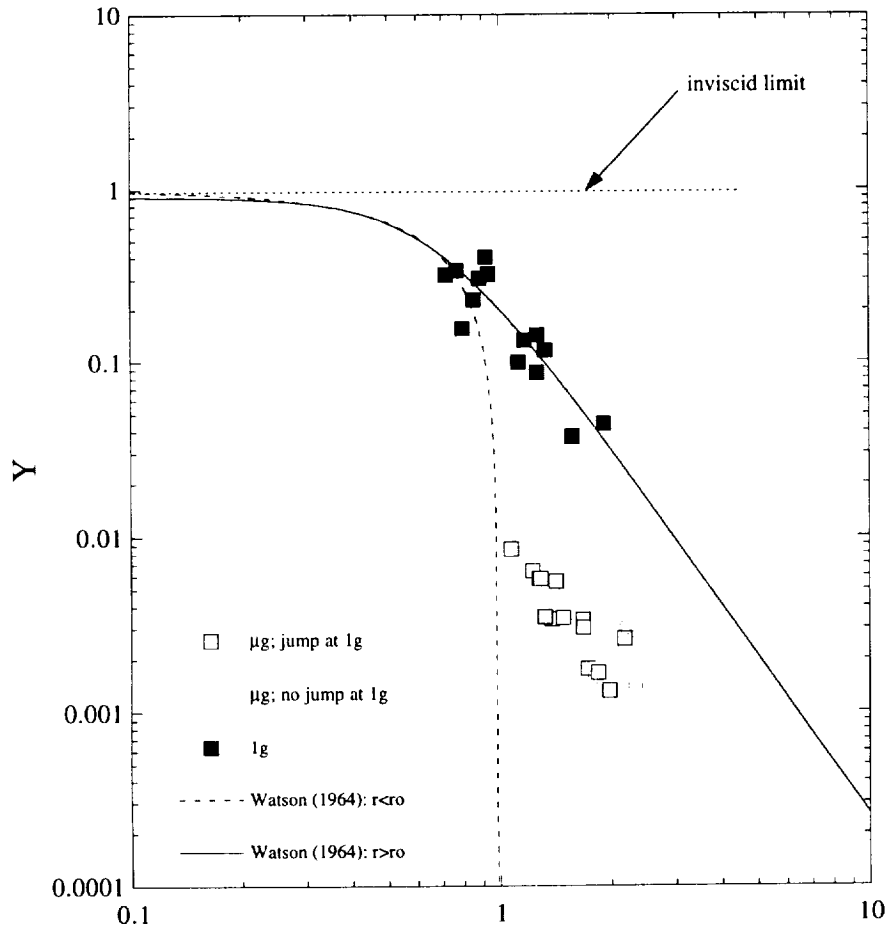


figure 14



R
Figure 15